

RSC Advances



This is an *Accepted Manuscript*, which has been through the Royal Society of Chemistry peer review process and has been accepted for publication.

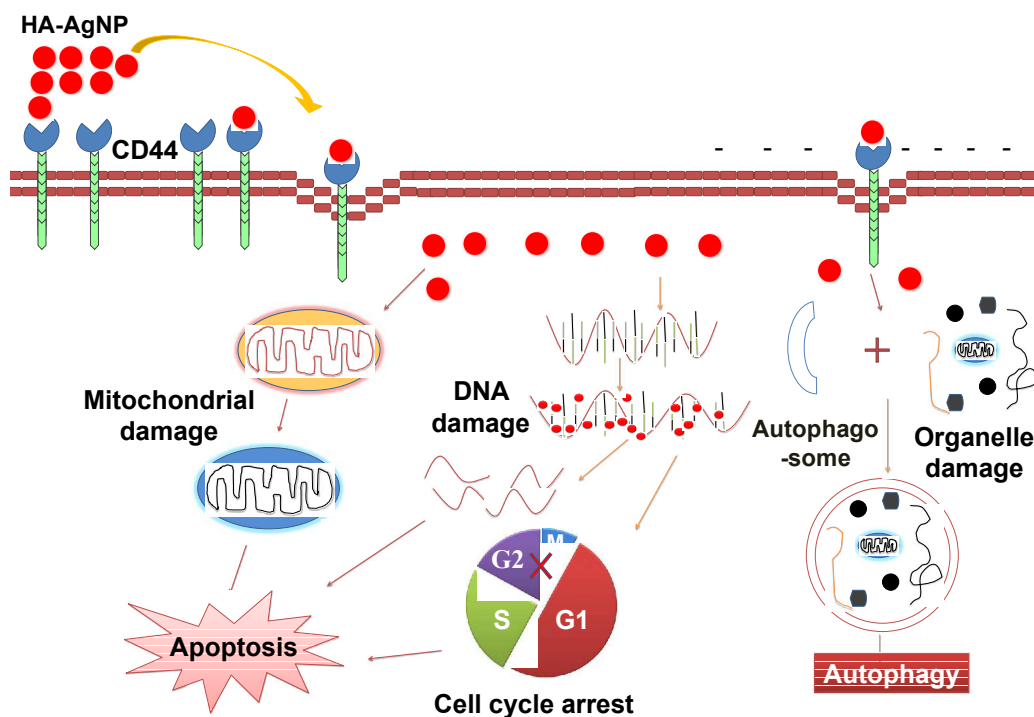
Accepted Manuscripts are published online shortly after acceptance, before technical editing, formatting and proof reading. Using this free service, authors can make their results available to the community, in citable form, before we publish the edited article. This *Accepted Manuscript* will be replaced by the edited, formatted and paginated article as soon as this is available.

You can find more information about *Accepted Manuscripts* in the [Information for Authors](#).

Please note that technical editing may introduce minor changes to the text and/or graphics, which may alter content. The journal's standard [Terms & Conditions](#) and the [Ethical guidelines](#) still apply. In no event shall the Royal Society of Chemistry be held responsible for any errors or omissions in this *Accepted Manuscript* or any consequences arising from the use of any information it contains.

Graphic abstract

A novel hyaluronic acid (HA)-based strategy for green synthesis of AgNP was developed, in which HA was used as both the reducer and stabilizer, and the HA-modified AgNP can target to the CD44-overexpressed cancer cells for improved therapy.



ARTICLE

Green Synthesis of Hyaluronic Acid-based Silver Nanoparticle and Its Enhanced Delivery to CD44⁺ Cancer Cells

Cite this: DOI: 10.1039/x0xx00000x

Received 00th January 2012,
Accepted 00th January 2012

DOI: 10.1039/x0xx00000x

www.rsc.org/

Jianming Liang,^{a,b†} Feng Zeng,^{a,b†} Meng Zhang,^a Zhenzhen Pan,^{a,c} Yingzhi Chen,^a Yuaner Zeng,^c Yong Xu,^d Qin Xu,^{*b} and Yongzhuo Huang^{*a}

The potent antitumor activities of silver nanoparticles (AgNP) have attracted great attention. However, the application of AgNP is restricted by its non-specific delivery and poor cellular uptake. We developed a novel hyaluronic acid (HA)-based strategy for green synthesis of AgNP, in which HA was used as the reducing agent and stabilizer. More importantly, HA is the ligand of CD44, and the HA-modified AgNP can target to CD44 receptors that are overexpressed in many types of cancer cells. The CD44-dependent endocytosis can significantly increase the intracellular delivery of HA-AgNP, compared to the non-modified one. The antitumor efficacy was significantly improved by HA modification. Furthermore, we found that multiple mechanisms were involved for the enhanced anticancer activities of HA-AgNP, including the decline of mitochondrial membrane potential, cell-cycle arrest and pyknosis, apoptosis, and autophagy. The HA-based strategy on green synthesis and CD44-targeting delivery provided a promising solution for AgNP-mediated cancer treatment.

Introduction

Silver had been applied empirically in water sterilization and food preservation for centuries and even millennia, long before humans knowing and finding microbes. Nevertheless, its official approval for medical use dates back to 1920s, when colloidal silver was accepted by the US FDA for wound therapy as an antibacterial agent.¹ Recently, the potent antitumor activities of AgNP have attracted great attention. AgNP induced cytotoxic effect against many types of cancer cells.² AgNP could produce intracellular reactive oxygen species (ROS) and cause progressive oxidative damage.³ Excess ROS generation significantly decreased mitochondrial functions.⁴ Besides, AgNP caused inhibition of chromosome segregation,⁵ DNA damage and cell cycle arrest,^{6,7} which indicated the cellular nuclei might be a possible target site. Nano-silver could also act against angiogenesis,⁸ and trigger programmed cell death.^{9, 10} More interestingly, AgNP could also efficiently kill the drug resistant cancer cells, due to the size-exclusion effect to evade drug efflux.¹¹

Despite the unique anticancer potential, lack of specific delivery and effective cellular uptake is a major drawback against the therapeutic application of AgNP. How to improve tumor and intracellular delivery is an important issue waiting to be solved for AgNP-based therapy.

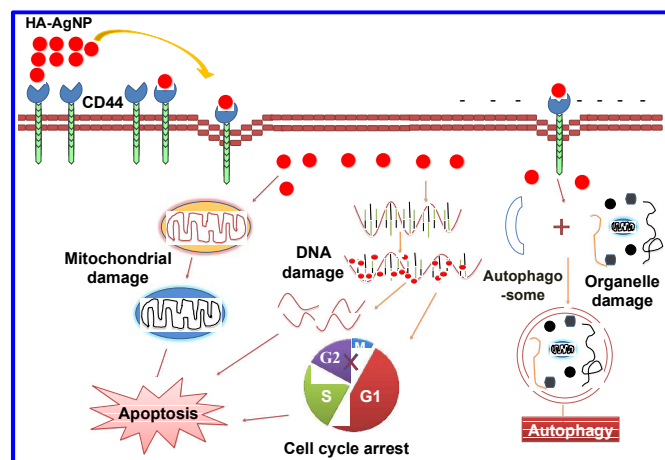
Hyaluronic acid (HA) is the naturally occurring polysaccharides with advantages of good biodegradability and non-toxicity, thus being commonly used for medical purpose. More attractively, HA is the principal ligand of CD44.¹² The receptor-ligand interaction of CD44/HA mediates the efficient internalization of HA.¹³ CD44 is overexpressed in many types of tumors, such as human lung cancer,¹⁴ breast cancer,¹⁵ colon cancer,^{16,17} and some multidrug-resistant carcinoma.^{18,19} Consequently, HA has been explored for use in drug delivery targeting to tumor.^{20,21}

We developed a novel HA-modified AgNP (HA-AgNP) for improved cancer therapy. We established a green method for AgNP synthesis, which was characterized that the aminated HA multi-functioned as both the targeting ligand and the reducing agent and stabilizer. The anti-tumor activities of the HA-AgNP were evaluated in the CD44⁺ colon carcinoma SW480 cells, as well as the human breast carcinoma MCF-7 cells. The impact of the HA-AgNP on the cell cycle, mitochondria, apoptosis, and autophagy was investigated. A possible mechanism of drug action was proposed as shown in **Scheme 1**.

Experimental details

Materials

HA with average molecular weight of 100 kDa was purchased from Qufu Liyang Biochem Co., Ltd. (Shandong, China). 1-Ethyl-3 (3-dimethylaminopropyl) carbodiimide (EDC), *N*-Hydroxysuccinimide (NHS) and silver nitrate were purchased from Sinopharm Chemical Reagent Co., Ltd. (Shanghai, China); pentaethylenehexamine from Heowns Biochemistry Co., Ltd. (Tianjin, China); JC-1 dye from Beijing Fanbo Science and Technology Co., Ltd. (Beijing, China); monodansylcadaverine (MDC) from Sigma-Aldrich (Saint Louis, Missouri, USA); propidium iodide and Hoechst 33342 from J&K Scientific (Beijing, China); Annexin V-FITC from BioVision Inc. (Mountain View, CA, USA); anti-CD44 antibodies from Abcam, Inc. (Cambridge, MA, USA). All other chemicals were of analytical grade and used without further purification.



Scheme. 1 The possible mechanisms of the antitumor effect of HA-AgNP.

Cell lines

The cell lines included human breast cancer MCF-7 and colon adenocarcinoma cell SW480 were obtained from the Cell Bank of the Chinese Academy of Sciences (Shanghai, China).

Methods

Synthesis of aminated hyaluronic acid The method was modified from a previous report.²² In brief, 500 mg HA was dissolved in water at a concentration of 10 mg/ml. Pentaethylenehexamine was added to the HA solution with a 30-fold molar excess. The pH of the reaction solution was adjusted to 5 with 1 M HCl. EDC and NHS (3 g each) were added to the reaction mixture. The reaction was allowed to proceed for 24 h, and at the reaction endpoint the pH was adjusted to 7 with 1 M NaOH. The thus-formed aminated HA was purified by exhaustive dialysis (MWCO 14,000) for 12 h against 25% ethanol solution, then 12 h against 0.1 M NaCl solution, and finally 48 h against ultrapure water. The solution was then centrifuged, and the supernatant lyophilized. The percentage of amino group substitution in HA was quantified by TNBS assay.^[23]

Synthesis of HA-AgNP and AgNP The aminated HA was dissolved in water at a concentration of 10 mg/ml. AgNO₃ (5-fold molar excess over the amino content) was added to the HA solution. The reaction solution was incubated at 37 °C for 12 h, and then dialyzed for 24 h against water. The HA-AgNP was thus obtained.

The synthesis procedures of AgNP were described as follows.²⁴ Eight milligrams of AgNO₃ were dissolved in 40 ml water. To the AgNO₃ solution, the NaOH solution (400 μl, 5 mg/ml), NH₃ solution (1 ml, 0.5%), and sucrose solution (4 ml, 30 mg/ml) were dropwise added, successively. The reaction solution was stirred for 1 h at 100 °C. The thus-formed AgNP was purified by centrifugation and rinsed using water.

Characterization of HA-AgNP and AgNP The HA-AgNP and AgNP were characterized by the surface plasmon resonance. The particle size and zeta potential were measured by using a Zeta sizer Nano-ZS90 (Malvern, UK) with proper dilution in distilled water. The morphology of the nanoparticles was observed by transmission electron microscope (TEM) (JEOL JEM-1200EX, Japan). The concentrations of Ag in HA-AgNP and AgNP suspensions were determined by using the *O*-phenyldiamine method.²⁵ The modification rate of HA-AgNP was estimated by using thermo gravimetric analysis (TGA, Pyris 1, PerkinElmer, USA).

Cellular uptake assay The SW480 and MCF-7 cells were incubated with the FITC-HA-AgNP and SAMSA fluorescein labelled AgNP with for 4 h at 37 °C. Subsequently, the cells were thoroughly washed with PBS, and then treated with Hoechst 33342 for labeling the nucleus. The cellular uptake of was observed by fluorescence microscopy. Quantitative determination was conducted by using flow cytometry (Calibur, BD, USA).

Anti-proliferative activity The anti-tumor activity of HA-AgNP and AgNP was assessed by a standard MTT assay. Briefly, the MCF-7 and SW480 cells were exposed to various concentrations of HA-AgNP or AgNP for 48 h, followed by MTT assay. The cell viability was calculated as the following formula:

$$\text{Cell viability (\%)} = \frac{OD_{\text{experimental group}}}{OD_{\text{control group}}} \times 100\%$$

Mitochondrial membrane potential (MMP) analysis MMP was investigated by using the fluorescent lipophilic cationic dye JC-1. The cells were treated with PBS, HA-AgNP and AgNP (58.5 μM Ag) for 24 h. The cells were collected, and then treated with the JC-1 solution (5 μg/ml) at 37 °C for 20 min. Subsequently, the cells were washed with PBS, and then subject to flow cytometry assay.

Cell Cycle Analysis Cell cycle analysis was based on measuring the DNA content by staining with propidium iodide (PI). The MCF-7 and SW480 cells were treated with PBS, HA-AgNP and AgNP (58.5 μM Ag) for 24 h. The cells were

harvested and fixed using cold 70% ethanol. The fixed cells were stained with the PI solution (50 $\mu\text{g/ml}$ PI, 0.1% Triton X-100, 37 $\mu\text{g/ml}$ EDTA and 50 $\mu\text{g/ml}$ RNase A) in the dark at 37 $^{\circ}\text{C}$ for 30 min. The samples were analyzed by flow cytometry.

Apoptosis assay The MCF-7 and SW480 cells were exposed to PBS, HA-AgNP and AgNP (58.5 μM Ag) for 48 h. The cells were stained with Hoechst 33342 (5 $\mu\text{g/ml}$) and PI (5 $\mu\text{g/ml}$) at 37 $^{\circ}\text{C}$ for 30 min. After wash with PBS for three times, the apoptotic cells were detected by fluorescence microscopy.

Similarly, after drugs treatment, the cells were stained with Annexin V-FITC/PI, and measured by flow cytometry.

Autophagy assay The MCF-7 and SW480 cells were treated with PBS, HA-AgNP and AgNP, same as in the section above. After removal of the medium, the cells were stained with the auto-fluorescent dye MDC (5 $\mu\text{g/ml}$) at 37 $^{\circ}\text{C}$ for 30 min. The cells were then washed three times with PBS. The autophagic vacuoles were immediately analyzed by fluorescence microscopy. Quantitative determination was conducted by using flow cytometry.

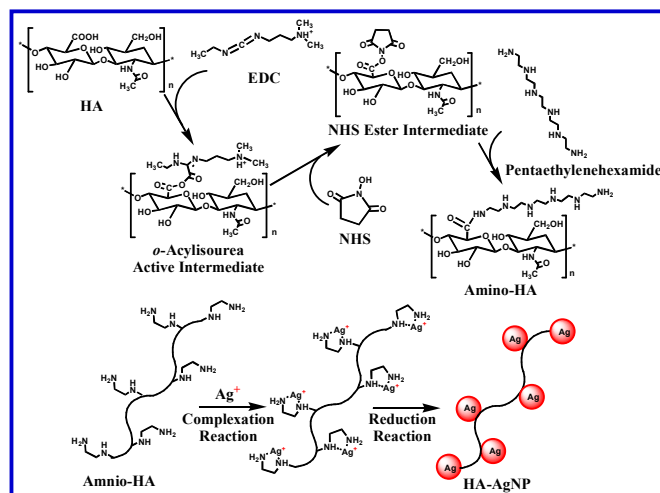
Interaction between HA-AgNP and CD44 The SW480 cells were treated with the FITC-HA-AgNP, and then washed three times with PBS, and fixed with 4% paraformaldehyde. The cells were incubated with anti-CD44 antibody (1/100) at 4 $^{\circ}\text{C}$ for 12 h, and Alexa Fluor 647-conjugated anti-rabbit IgG (1/100) was used as the secondary antibody. The slides were incubated in the dark at 37 $^{\circ}\text{C}$ for 1 h. After thorough wash with PBS, the cells were observed by using confocal laser scanning microscopy (Olympus FV1000, Japan).

Furthermore, the receptor-mediated endocytosis of HA-AgNP was investigated by the competitive inhibition experiment. In brief, the SW480 cells were incubated with free HA (1 mg/ml) for 1 h at 37 $^{\circ}\text{C}$. Then the FITC-HA-AgNP was added to the cells. After 4 h treatment, the cells were harvested and washed three times by the PBS, and then measured by flow cytometry.

Results and discussion

Chemical reduction is the most common method for AgNP preparation. The principle of this method is that a soluble silver salt is reduced to the silver nanoparticles in the presence of the reductants,²⁶ such as sodium borohydride and hydrazine hydrate.^{27,28} These agents, however, are toxic. In addition, stabilizers are required to maintain the colloidal stability, but hazardous surfactants (e.g., cetrimonium bromide, CTAB) are often used. With the rise of green chemistry, the eco-friendly and biodegradable materials from the natural products, such as polysaccharides, have been applied in the synthesis of AgNP.^{29,30} We developed a green method for AgNP preparation by using the biocompatible HA as both a reductant and stabilizer.

The preparation process of HA-AgNP is illustrated in **Scheme 2**. Amination rate of HA was calculated to be 40%. Because of the reducing activity of HA, Ag^+ was turned into silver nanocrystal that was subsequently stabilized by the hydrophilic HA, and thus formed the nanoparticulate clusters.



Scheme 2 Synthetic schemes and structures of HA-AgNP.

Surface plasmonic properties of AgNP have been widely used for characterization.³¹ The spectral response of the HA-AgNP and AgNP are shown in **Fig. 1a**. The absorption peak of HA-AgNP and AgNP were at 422 and 432 nm, respectively. The surface plasmon absorbance typically falls in the range of 400–450 nm.³² The weight loss during heating up to 750 $^{\circ}\text{C}$ was monitored by TGA (**Fig. 1b**). The TGA curve shows that the weight loss of the aminated HA alone was 79.7% while the HA-AgNP was 66.6%. The 13.1% in weight loss change was due to the formation of AgNP. Of note, the remaining ash in HA could be accounted for residual Na_2CO_3 .³³ The morphology of AgNP and HA-AgNP was observed by using TEM (**Fig. 1c**). The observation was in accordance with the measurement by dynamic light scattering. The mean particle size, polydispersity index (PDI), and zeta potential of HA-AgNP and AgNP are given in **Table 1**. The mean size of HA-AgNP and AgNP were 305.5 and 60.9 nm, and the zeta potential +17.3 and -10.3 mV, respectively. The positive zeta potential of HA-AgNP may be related to the amine residues and the complexation between amine groups and Ag^+ .

Table 1 Particle size, PDI and zeta potential measurements.

	Particle size (nm)	PDI	Zeta potential (mV)
AgNP	60.9±2.4	0.24±0.02	-10.3±0.6
HA-AgNP	305.5±15.1	0.33±0.03	+17.3±0.9

(Each represents the mean \pm SD of $n = 3$)

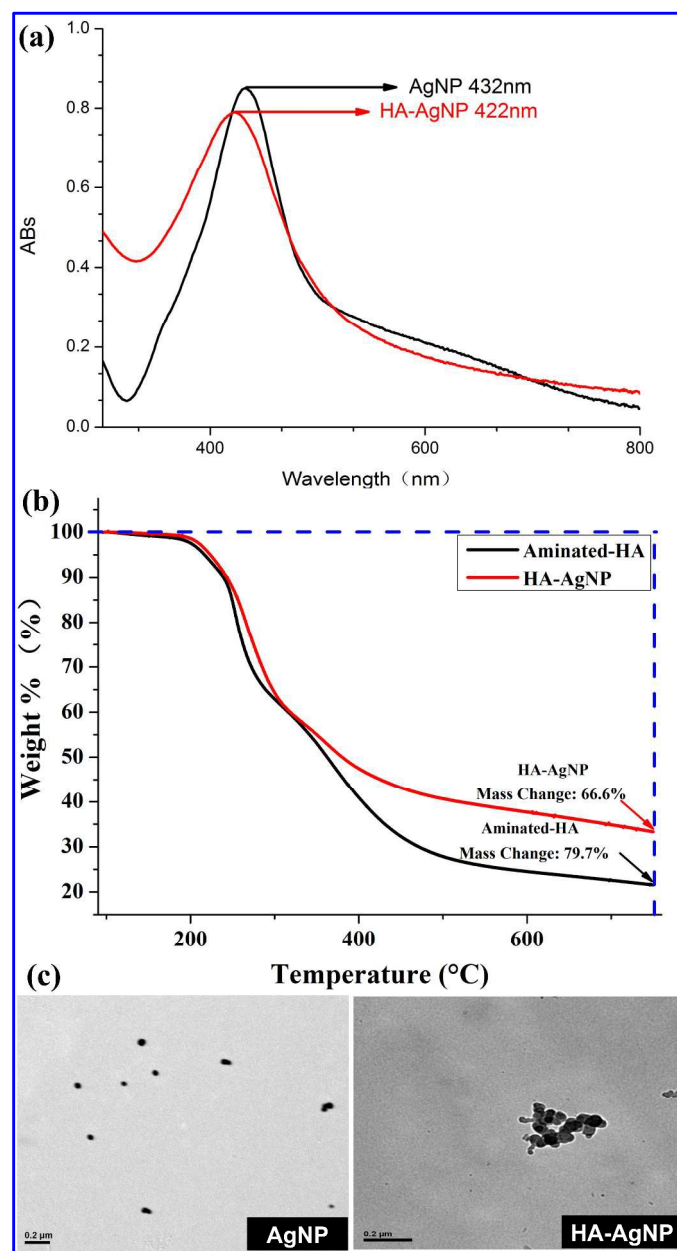


Fig. 1 (a) UV-visible spectra of HA-AgNP and AgNP. (b) TGA curves of HA-AgNP and AgNP. (c) TEM imaging of HA-AgNP and AgNP.

It has been well demonstrated that SW480 cells overexpressed CD44,³⁴ while MCF-7 cells showed minor expression.³⁵ Therefore, the MCF-7 and SW480 cells were selected in our studies. As expected, the cellular uptake of HA-AgNP was significantly higher in SW480 cells than in MCF-7 cells (**Fig. 2a-c**), related to their CD44 expression levels (**Fig. 2d**). By contrast, AgNP showed very low cellular uptake in both cell lines. The mechanisms responsible for cellular uptake of AgNP may account for the endocytosis,³⁶ such as clathrin-dependent endocytosis and macropinocytosis.³⁷ The uptake efficiency by this pathway, however, was not sufficient.

Cell viability was investigated by MTT assay. HA-AgNP efficiently inhibited the proliferation of MCF-7 and SW480 cells, with IC_{50} of 24.6 and 20.7 μ M, respectively, but AgNP showed little cytotoxicity to the cells at the same tested concentrations as HA-AgNP (**Fig. 3a-b**). It should be mentioned that HA-AgNP displayed better biocompatibility to the non-tumoral cells (i.e., human umbilical vein endothelial cells, HUVEC), compared with CTAB-AgNP prepared with the conventional reductant and stabilizer (sodium borohydride and CTAB) (**Fig. 3c**).

Our results showed that CD44 receptor-mediated endocytotic pathway significantly enhanced the HA-AgNP intracellular delivery and its antitumor activity accordingly.

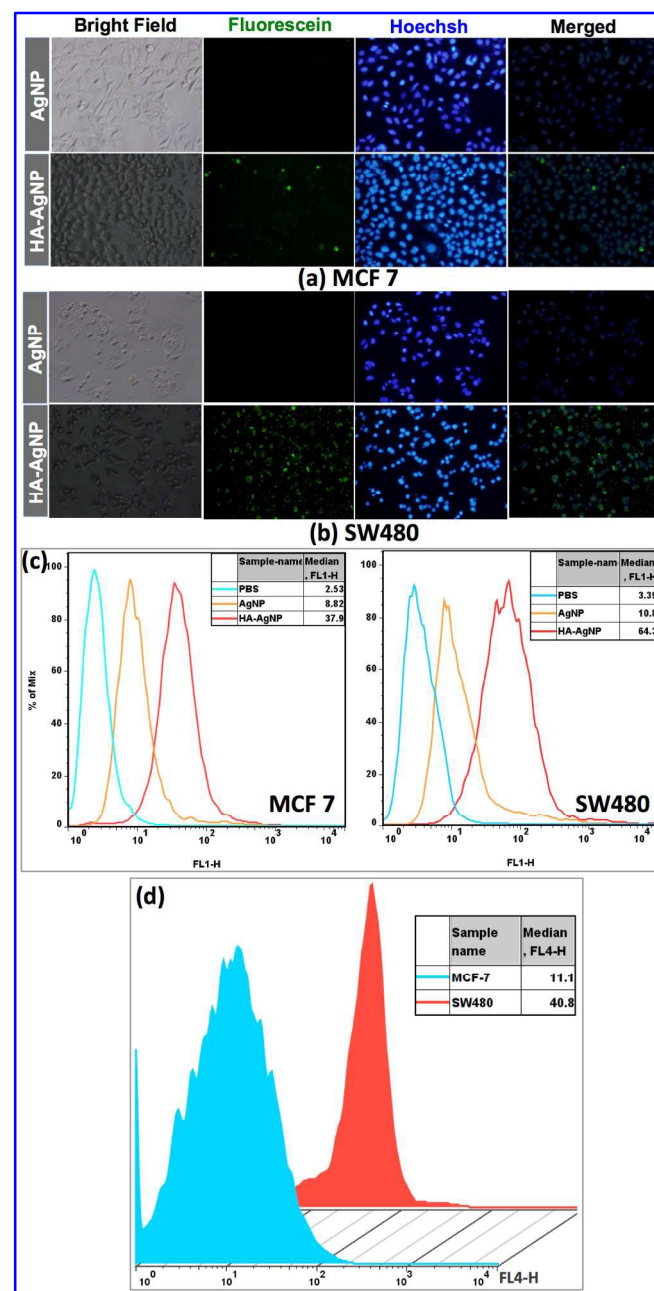


Fig. 2 Cellular uptake of HA-AgNP and AgNP in MCF-7 (a) and SW480 cells (b) (200 \times). (c) Flow cytometry assay of the AgNP and HA-AgNP cellular uptake in MCF-7 and SW480 cells. (d) CD44 expression on MCF-7 and SW480 cells.

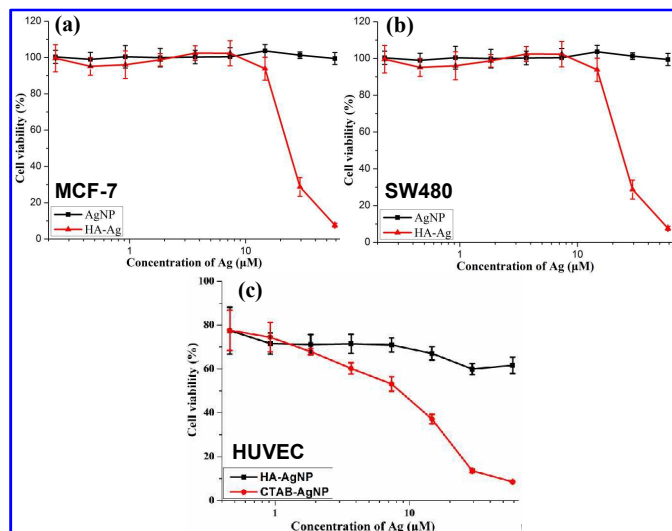


Fig. 3 Anti-tumor activity of AgNP and HA-AgNP on (a) MCF-7 and (b) SW480 cells. (c) Biocompatibility of HA-AgNP and CTAB-AgNP to HUVEC cells.

The mitochondrion is the powerhouse of the cell. After cell entry, AgNP could accumulate outside the mitochondria, impair mitochondrial functions and induce apoptosis.³⁸ The MMP can be used as an early marker of the onset of apoptosis.³⁹ When the mitochondrial membrane is in collapse, the JC-1 dye indicates the potential change by a fluorescence shift from red to green, which is related to the change from highly energized mitochondria to low voltage mitochondria. This shift provides a quantitative index of apoptosis for use in the flow cytometry.⁴⁰ The ratio of cells with MMP was measured to be 50.9% for MCF-7 and 71.3% for SW480 cells after treatment with HA-AgNP (**Fig. 4**), but in the AgNP group there were only 15.3% and 30.2% in these two cell lines, respectively. The significant increase in MMP implied the mitochondria injury caused by HA-AgNP, compared with AgNP.

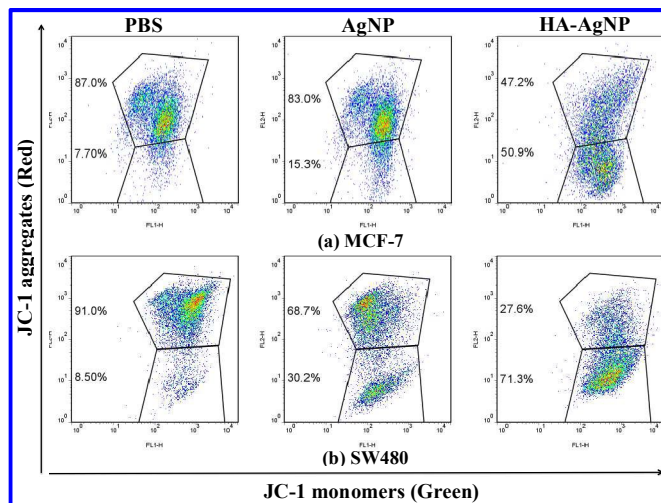


Fig. 4 Bivariate JC-1 analysis of mitochondrial membrane potential in (a) MCF-7 and (b) SW480 cells by flow cytometry.

The influence of HA-AgNP and AgNP on the cell cycle was evaluated by measuring the DNA content using flow cytometry. Cell proliferation mainly includes the following phases: G1 phase (cell grows), S phase (DNA synthesis), G2 phase (cell prepares to division) and M phase (mitosis). The amount of nuclear DNA varies with the different phases, for example, diploid (2N) at G1, tetraploid (4N) at G2/M, and S-phase cells contain DNA amount varying between the G1 and G2. In addition, the DNA content in apoptotic cells is mostly less than 2N (the sub-G1 cells). After exposure to HA-AgNP, there was a significant increase in sub-G1 phase in the tumor cells, measured to be 16.4% and 15.6% in MCF-7 and SW480, respectively, whereas there was merely a slight increase in the AgNP-treated cells (**Fig. 5**). The results indicated the enhanced apoptosis induced by HA-AgNP compared with AgNP. Because nanosilver could bind with DNA and initiate DNA impair,^{41,42} the thus-released damage signals could induce apoptosis.⁴³

The cell death pattern was observed by using Hoechst 33342 and PI double staining. Hoechst 33342 is a cell-penetrating nucleic acid dye, while PI is a cell-impermeable dye that is used for labeling DNA of the apoptotic cells with increased plasma membrane permeability or lost of membrane integrity. Therefore, normal and apoptotic cell populations can be identified by fluorescence microscopy.⁴⁴ In addition, the translocation of phosphatidylserine (PS) from the inner side of the plasma membrane to the outer layer occurs in the early stages of apoptosis. Annexin V can bind with the exposed PS, and thus the Annexin V-FITC stained cells indicate early apoptosis.^{45,46}

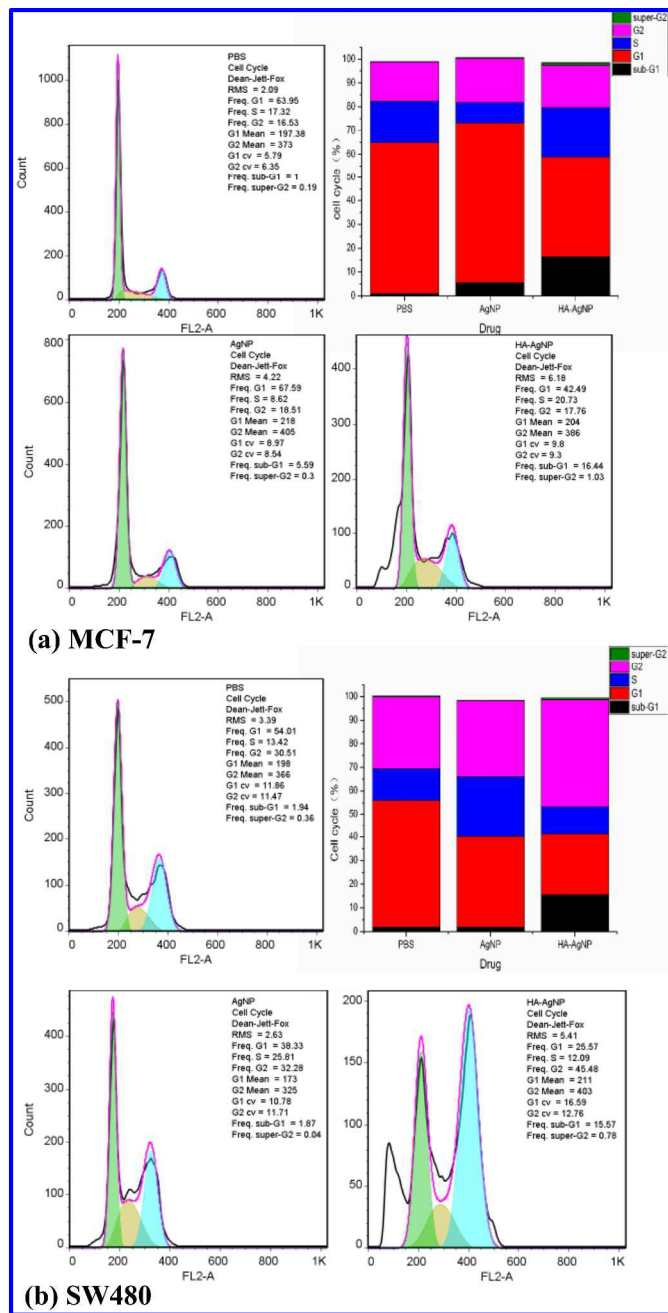


Fig. 5 Cell cycle analysis of MCF-7 (a) and SW480 cells (b) in the presence of HA-AgNP, AgNP, and PBS by flow cytometry.

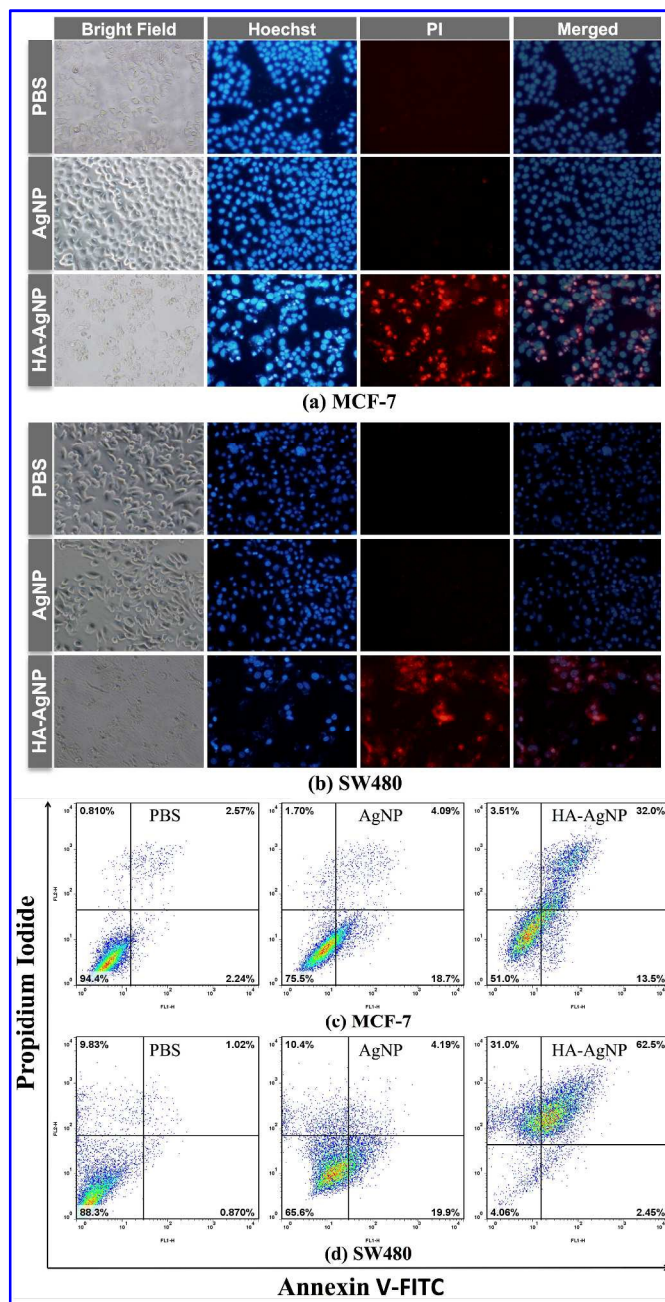


Fig. 6 Representative fluorescence photomicrographs show morphological changes of MCF-7 (a) and SW480 cells (b) detected by dual staining of Hoechst 33342/PI (200 \times). Bivariate annexin V/PI analysis of MCF-7 (c) and SW480 cells (d) after drug treatment.

In the PBS and AgNP groups, the MCF-7 and SW480 cells were in the typical oval shape (Fig. 6, bright field), and only showed blue fluorescence (Hoechst). On the contrary, typical apoptosis characteristics were observed in the HA-AgNP group, showing the decreased amount of cells and the increased formation of apoptotic bodies. The characteristics of apoptotic bodies included cell shrinkage, nuclear fragmentation and pyknosis. Owing to the lost of plasma membrane integrity, the

fragmented nuclei showed red fluorescence, indicating late apoptosis.

Similarly, the percentage of apoptotic cells was determined in the bivariate annexin V-FITC/PI analysis (Fig. 6c-d). The Annexin-V⁺/PI⁻ cells were identified as early apoptotic cells, and the Annexin-V⁺/PI⁺ dual positive cells were identified as late apoptotic cells. The PBS groups in both cells exhibited normal levels of staining (Annexin-V/PI⁻). Low levels of apoptosis were found after AgNP treatment, and only 18.7% and 19.9% of Annexin-V⁺/PI⁻ cells were detected in MCF-7 and SW480 cells, respectively. Furthermore, 13.5%/32.0% and 2.45%/62.5% early/late apoptotic cells were detected in MCF-7 and SW480 cells, respectively. The results indicated the close association between the significant increase of apoptotic rate in the HA-AgNP groups and the CD44 expression level on cell surface. The results were consistent with the previous experiments.

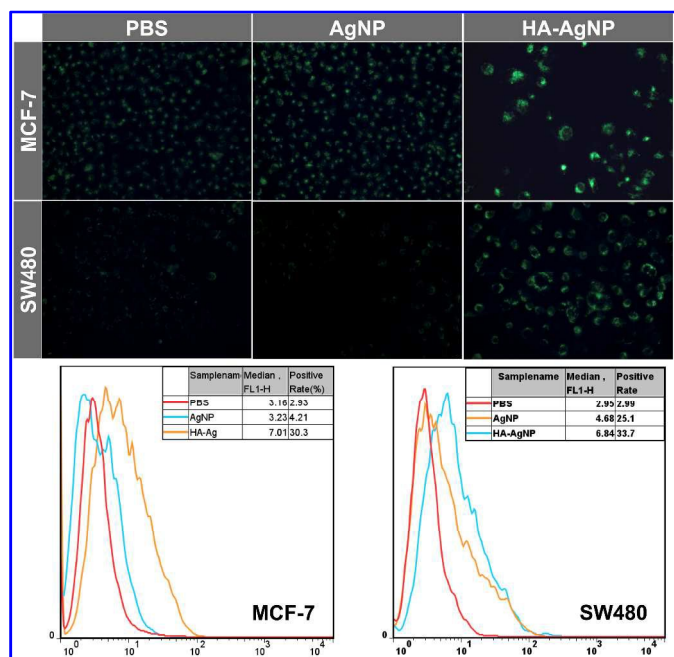


Fig. 7 Detection of autophagic vacuoles with drug treatment in MCF-7 and SW480 cells stained by MDC (200 \times) (top panel). Analysis of MDC positive vacuoles after drug exposure to MCF-7 and SW480 cells (bottom panel).

Autophagy is a critical regulator of cellular metabolism and homeostasis. The cells initiate autophagy under stress conditions such as hypoxia, starvation, high or low temperature and drug effects.⁴⁷ The stress conditions cause injury of organelles. In order to maintain cellular normal functions, the damaged organelles will be sequestered into autophagosomes and then delivered to the lysosome for degradation.⁴⁸ Autophagy-related protein 8 (Atg8) is an ubiquitin-like protein required for autophagosome formation. Monodansylcadaverine (MDC, green fluorescence) can specifically bind to the Atg8, and thus be used as an autophagolysosome marker.⁴⁹ The cells

with HA-AgNP treatment displayed the increased fluorescence and the autophagic vacuoles. The observation was further confirmed by the quantitative analysis of autophagosome by flow cytometry (Fig. 7). HA-AgNP significantly enhanced the formation of autophagolysosomes. As demonstrated in the studies above, HA-AgNP can cause damage in mitochondria and nuclei, and the damaged organelles would subsequently trigger autophagy as adaptive response to the HA-AgNP stress.

The interaction between HA-AgNP and CD44 was investigated in the SW480 cells. Confocal double-fluorescence images show co-localization of CD44 (green) and HA-AgNP (red), displaying the yellow color in the merged image (Fig. 8).

CD44 is responsible for the binding and uptake of HA. In order to examine the CD44-mediated endocytosis of HA-AgNP, free HA was added for saturating the CD44 receptors on cell surface. The cellular uptake of HA-AgNP in the presence of HA was significantly decreased owing to the competitive inhibition (Fig. 8, bottom panel).

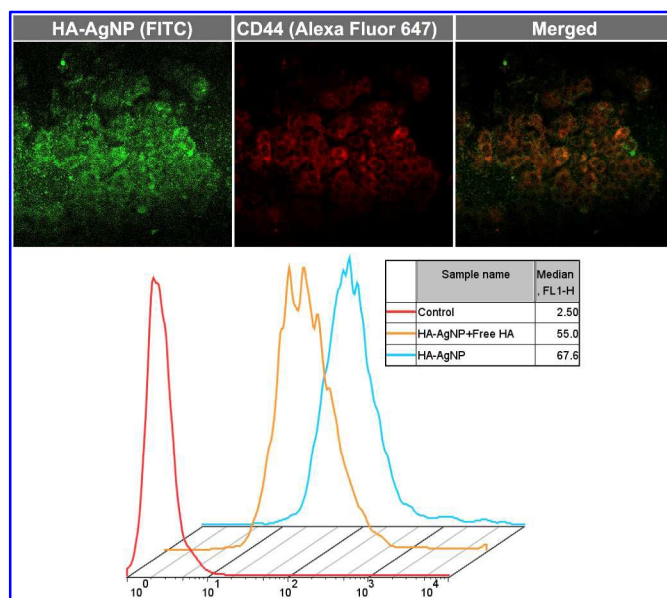


Fig. 8 Colocalization of CD44 receptor and HA-AgNP in the membrane of the SW480 cells (top panel). Flow cytometry assay of the cellular uptake of FITC-HA-AgNP in the presence (or absence) of free HA (bottom panel).

The HA-AgNP cellular uptake studies revealed that SW480 cells was higher than MCF-7 cells. HA-AgNP also showed increased cytotoxicity on SW480 compared to MCF-7 cells, and displayed more significant effect on MMP and apoptosis in SW480 than in MCF-7 cells. However, it must be pointed out that due to the distinct natures (e.g., the sensitivity to a specific cytotoxic agent) between different cell lines, it is difficult to connect the cytotoxicity results with the CD44 expression levels. Therefore, it would be more reasonable to compare the results from the same cell line, for instance, the competitive inhibition

studies on SW480 cells in which the cellular uptake of HA-AgNP was reduced in the presence of HA, providing evidence of the CD44-mediated internalization pathway.

Conclusion

In summary, a novel method for green synthesis of AgNP was developed based on the aminated HA that can multi-function as the reducing agent and stabilizer, as well as a targeting ligand. The HA-AgNP could benefit from the CD44-mediated endocytosis, which thus enhances delivery to the CD44⁺ cancer cells. Accordingly, the antitumor efficacy of HA-AgNP was significantly enhanced, in comparison with the non-modified AgNP. The improved anticancer activities could involve multiple mechanisms including the cell-cycle arrest, mitochondrial membrane potential decline, apoptosis, and autophagy. The HA-based strategy on green synthesis and CD44-targeting delivery provided a promising solution for AgNP application in cancer treatment.

Acknowledgements

This work was supported by 973 Program, China (2014CB931900, 2013CB932503) and NSFC, China (81172996, 81373357, 81422048).

Notes and references

^a Shanghai Institute of Materia Medica, Chinese Academy of Sciences, 501 Hai-ke Rd, Shanghai 201203, China. Email: yzhuang@simm.ac.cn; Fax: +86 21 2023-1981; Tel: +86 21 2023-1000 ext. 1401.

^b Guangzhou University of Chinese Medicine, Tropical Medicine Institute, Guangzhou 501450, China. Email: xuqin@163.com

^c Guangzhou University of Chinese Medicine, School of Chinese Materia Medica, Guangzhou 501450, China.

^d Hubei Biological Medicine Industrial Technological Institute Co., Ltd Wuhan 430075, China.

† Equal contribution.

1. I. Chopra, *J. Antimicrob. Chemother.*, 2007, **59**, 587-590.
2. Z. Huang, X. Jiang, D. Guo and N. Gu, *J. Nanosci. Nanotechnol.*, 2011, **11**, 9395-9408.
3. R. Foldbjerg, D. A. Dang and H. Autrup, *Arch. Toxicol.*, 2011, **85**, 743-750.
4. D. Guo, L. Zhu, Z. Huang, H. Zhou, Y. Ge, W. Ma, J. Wu, X. Zhang, X. Zhou and Y. Zhang, *Biomaterials*, 2013, **34**, 7884-7894.
5. P. D. Nallathamby and X.-H. N. Xu, *Nanoscale*, 2010, **2**, 942-952.
6. M. I. Sriram, S. B. M. Kanth, K. Kalishwaralal and S. Gurunathan, *Int. J. Nanomed.*, 2010, **5**, 753.
7. P. AshaRani, G. Low Kah Mun, M. P. Hande and S. Valiyaveetil, *ACS nano*, 2008, **3**, 279-290.
8. S. Gurunathan, K.-J. Lee, K. Kalishwaralal, S. Sheikpranbabu, R. Vaidyanathan and S. H. Eom, *Biomaterials*, 2009, **30**, 6341-6350.
9. P. Sanpui, A. Chattopadhyay and S. S. Ghosh, *ACS Appl. Mater. Interfaces*, 2011, **3**, 218-228.

10. N. K. Verma, J. Conroy, P. E. Lyons, J. Coleman, M. P. O'Sullivan, H. Kornfeld, D. Kelleher and Y. Volkov, *Toxicol. Appl. Pharmacol.*, 2012, **264**, 451-461.
11. J. Liu, Y. Zhao, Q. Guo, Z. Wang, H. Wang, Y. Yang and Y. Huang, *Biomaterials*, 2012, **33**, 6155-6161.
12. T. Ahrens, V. Assmann, C. Fieber, C. C. Termeer, P. Herrlich, M. Hofmann and J. C. Simon, *J. Invest. Dermatol.*, 2001, **116**, 93-101.
13. W. Knudson, G. Chow and C. B. Knudson, *Matrix Biol.*, 2002, **21**, 15-23.
14. M. Yasuda, Y. Tanaka, K. Fujii and K. Yasumoto, *Int. Immunol.*, 2001, **13**, 1309-1319.
15. G. Tzircotis, R. F. Thorne and C. M. Isacke, *J. Cell Sci.*, 2005, **118**, 5119-5128.
16. C. Wang, J. Xie, J. Guo, H. C. Manning, J. C. Gore and N. Guo, *Oncol. Rep.*, 2012, **28**, 1301-1308.
17. G.h. Rao, H.m. Liu, B.w. Li, J.j. Hao, Y.l. Yang, M.r. Wang, X.h. Wang, J. Wang, H.j. Jin and L. Du, *Acta Pharmacol. Sin.*, 2013, **34**, 793-804.
18. X. J. Fang, H. Jiang, Y. Q. Zhu, L. Y. Zhang, Q. H. Fan and Y. Tian, *Oncol. Rep.*, 2014, **31**, 2735-2742.
19. P. Van Phuc, P. L. C. Nhan, T. H. Nhung, N. T. Tam, N. M. Hoang, V. G. Tue, D. T. Thuy and P. K. Ngoc, *Onco Targets Ther.*, 2011, **4**, 71.
20. D. Coradini, S. Zorzet, R. Rossin, I. Scarlata, C. Pellizzaro, C. Turrin, M. Bello, S. Cantoni, A. Speranza and G. Sava, *Clin. Cancer Res.*, 2004, **10**, 4822-4830.
21. S. Ganesh, A. K. Iyer, D. V. Morrissey and M. M. Amiji, *Biomaterials*, 2013, **34**, 3489-3502.
22. E. J. Oh, K. Park, K. S. Kim, J. Kim, J.-A. Yang, J.-H. Kong, M. Y. Lee, A. S. Hoffman and S. K. Hahn, *J. Control. Release*, 2010, **141**, 2-12.
23. H. Tan, C. M. Ramirez, N. Miljkovic, H. Li, J. P. Rubin and K. G. Marra, *Biomaterials*, 2009, **30**, 6844-6853.
24. E. Filippo, A. Serra, A. Buccolieri and D. Manno, *J. Non-Cryst. Solids*, 2010, **356**, 344-350.
25. B. Anilnert, G. Yalçin, F. Ariöz and E. Dölen, *Anal. Lett.*, 2001, **34**, 113-123.
26. X. Z. Lin, X. Teng and H. Yang, *Langmuir*, 2003, **19**, 10081-10085.
27. D. L. Van Hying and C. F. Zukoski, *Langmuir*, 1998, **14**, 7034-7046.
28. K. Do Kim, D. N. Han and H. T. Kim, *Chem. Eng. J.*, 2004, **104**, 55-61.
29. X. Cao, C. Cheng, Y. Ma and C. Zhao, *J. Mater. Sci. Mater. Med.*, 2010, **21**, 2861-2868.
30. Y. Liu, S. Chen, L. Zhong and G. Wu, *Radiat. Phys. Chem.*, 2009, **78**, 251-255.
31. V. Amendola, O. M. Bakr and F. Stellacci, *Plasmonics*, 2010, **5**, 85-97.
32. T. Abdul Kareem and A. Anu Kaliani, *Arab. J. Chem.*, 2011.
33. J. Soares, J. Santos, G. Chierice and E. Cavalheiro, *Eclética Química*, 2004, **29**, 57-64.
34. G. Rao, H. Wang, B. Li, L. Huang, D. Xue, X. Wang, H. Jin, J. Wang, Y. Zhu and Y. Lu, *Clin. Cancer Res.*, 2013, **19**, 785-797.
35. C. Surace, S. Arpicco, A. Dufay-Wojcicki, V. Marsaud, C. Bouclier, D. Clay, L. Cattel, J.-M. Renoir and E. Fattal, *Mol. Pharm.*, 2009, **6**, 1062-1073.

36. S. Kittler, C. Greulich, J. Diendorf, M. Koller and M. Epple, *Chem. Mater.*, 2010, **22**, 4548-4554.
37. C. Greulich, J. Diendorf, T. Simon, G. Eggeler, M. Epple and M. Köller, *Acta Biomater.*, 2011, **7**, 347-354.
38. E. Bressan, L. Ferroni, C. Gardin, C. Rigo, M. Stocchero, V. Vindigni, W. Cairns and B. Zavan, *Int. J. Dent.*, 2013, **2013**, 312747
39. S. Hunot and R. A. Flavell, *Science*, 2001, **292**, 865-866.
40. P. X. Petit, H. Lecoœur, E. Zorn, C. Daguët, B. Mignotte and M.-L. Gougeon, *J. Cell Biol.*, 1995, **130**, 157-167.
41. W. Yang, C. Shen, Q. Ji, H. An, J. Wang, Q. Liu and Z. Zhang, *Nanotechnol.*, 2009, **20**, 085102.
42. S. Hackenberg, A. Scherzed, M. Kessler, S. Hummel, A. Technau, K. Froelich, C. Ginzkey, C. Koehler, R. Hagen and N. Kleinsasser, *Toxicol. Lett.*, 2011, **201**, 27-33.
43. A. Tyagi, C. Agarwal, G. Harrison, L. M. Glode and R. Agarwal, *Carcinogenesis*, 2004, **25**, 1711-1720.
44. S. N. Syed Abdul Rahman, N. Abdul Wahab and S. N. Abd Malek, *Evid. Based Complement. Alternat. Med.*, 2013, **2013**.
45. S. Martin, C. Reutellingsperger, A. J. McGahon, J. A. Rader, R. Van Schie, D. M. LaFace and D. R. Green, *J. Exp. Med.*, 1995, **182**, 1545-1556.
46. I. Vermes, C. Haanen, H. Steffens-Nakken and C. Reutellingsperger, *J. Immunol. Methods*, 1995, **184**, 39-51.
47. A. Biederbick, H. Kern and H. Elsässer, *Eur. J. Cell Biol.*, 1995, **66**, 3-14.
48. A. L. Contento, Y. Xiong and D. C. Bassham, *Plant J.*, 2005, **42**, 598-608.
49. G. Kroemer, G. Mariño and B. Levine, *Mol. Cell*, 2010, **40**, 280-293.